DOI: 10.1002/ejic.201000251

# Nanostructures of Metal Tellurides (PbTe, CdTe, $CoTe_2$, $Bi_2Te_3$, and $Cu_7Te_4$) with Various Morphologies: A General Solvothermal Synthesis and Optical Properties

**Ling Jiang,[a] Ying-Jie Zhu,*[a] and Jing-Biao Cui[b]**

**Keywords:** Tellurium / Nanostructures / Self-assembly / Luminescence / Reaction mechanisms

A general surfactant-assisted solvothermal route was developed for the synthesis of a variety of metal telluride nanostructures. In this method, a corresponding metal salt, $Na_2TeO_3$, ascorbic acid, and polyvinyl pyrrolidone (PVP) were used as reagents and a mixture of ethylene glycol (EG) and water was used as the solvent. The synthesis of nanostructures including PbTe, CdTe, $CoTe_2$, $Bi_2Te_3$, and $Cu_7Te_4$ with varied morphologies was demonstrated by using this general approach. The mechanisms of formation of these telluride nanostructures are discussed. The optical properties including UV/Vis absorption of $Cu_7Te_4$ and CdTe and photoluminescence of $CoTe_2$ nanostructures are investigated.

## Introduction

One-dimensional (1D) nanostructures, including nanotubes, nanowires, and nanorods, are hot research topics and are intensively studied due to their novel properties and potential applications in electronics and optoelectronics.[1] Among various interesting nanomaterials, metal tellurides have their own distinctive properties such as a high Seebeck coefficient observed in PbTe. This remarkable property in combination with low thermal conductivity and high electrical conductivity has made PbTe and its alloys attractive materials for refrigeration and electrical power generation from heat.[2,3] Theoretical investigations suggest that $Bi_2Te_3$ nanowires may exhibit ZT values much larger than 1.0, resulting from both the enhanced thermoelectric power ($S$) and electrical conductivity ($\sigma$) and depressed thermal conductivity ($\kappa$) in the nanostructures.[4,5] Another typical example is cadmium telluride (CdTe), a near-infrared band-gap semiconductor ($E_g$ = 1.56 eV, 300 K) with novel optical and electrical properties, having been widely used for a variety of applications such as photovoltaic devices,[6] light-emitting diodes,[7] biological sensors,[8] and nanoscale electronics.[9] In contrast to the aforementioned metal tellurides, however, fewer studies on transition metal tellurides have been performed so far.[10] For example, there have been few investigations of $Cu_7Te_4$ nanostructures, a typical transition metal telluride. Li et al.[11] developed a solvothermal route for the synthesis of nanocrystalline $Cu_7Te_4$ at low temperature. They also used a room-temperature sonochemical route to successfully prepare nanocrystalline $Cu_7Te_4$ and $Cu_4Te_3$.[12] Similar to copper tellurides, another transition metal telluride $CoTe_2$ has not been well studied either. Xie et al.[13] prepared $CoTe_2$ nanorods by the reaction of $CoCl_2{\cdot}6H_2O$ and tellurium in ethylenediamine by a solvothermal method. To the best of our knowledge, little is known about the optical properties of the transition metal telluride nanostructures.

Although a few techniques have been used to grow 1D metal telluride nanostructures, one universal and facile route to the synthesis of different types of metal telluride nanostructures has not been developed to this point. Furthermore, the two-step Te template-directed synthesis is one of the most popular strategies for the fabrication of 1D telluride nanostructures[14–17] and uses toxic and hazardous $N_2H_4{\cdot}H_2O$ as a common reducing agent.[14–22] Recently, we developed an environmentally benign method for the synthesis of PbS, PbSe, and PbTe nanotubes by using a biomolecule-assisted nanowire-templated route.[23] In terms of both fundamental understanding and practical applications, it is desirable to develop a general, one-step, less hazardous route to the synthesis of metal telluride nanostructures.

In this study, we developed a simple one-step solvothermal process to synthesize various metal telluride nanostructures. Five different types of telluride nanostructures (PbTe, CdTe, $CoTe_2$, $Bi_2Te_3$, and $Cu_7Te_4$) with various morphologies were synthesized by using this one general approach. It can be applied to synthesize other nanostructured telluride compounds. The optical properties of the CdTe, $CoTe_2$, and $Cu_7Te_4$ nanomaterials were also investigated.

[a] State Key Laboratory of High Performance Ceramics and Superfine Microstructure, Shanghai Institute of Ceramics, Chinese Academy of Sciences,
Shanghai 200050, P. R. China
Fax: +86-21-52413122
E-mail: y.j.zhu@mail.sic.ac.cn
[b] Department of Physics and Astronomy, University of Arkansas at Little Rock,
Little Rock, AR 72204, USA

  

## Results and Discussion

### Structural Characterization

Figure 1 shows a typical XRD pattern and TEM images of as-synthesized PbTe nanowires. The diffraction peaks in the XRD pattern (Figure 1a) can be readily indexed to a single phase of PbTe with a cubic structure (JCPDS No.78–1905). EDS was carried out on a single nanowire by using Cu grids as a sample carrier, and the data is plotted in Figure 1b. Both Pb and Te elements were detected and their atomic ratio was calculated to be approximately 1:1. This value confirms that PbTe was obtained, which is consistent with the XRD measurements. The morphology of the PbTe sample was investigated by TEM and is shown in Figure 1c,d. PbTe nanowires with an average diameter of 20 nm and lengths up to micrometers were observed. The nanowires have a uniform distribution in diameters. Note that most of the nanowires were curled instead of completely straight.

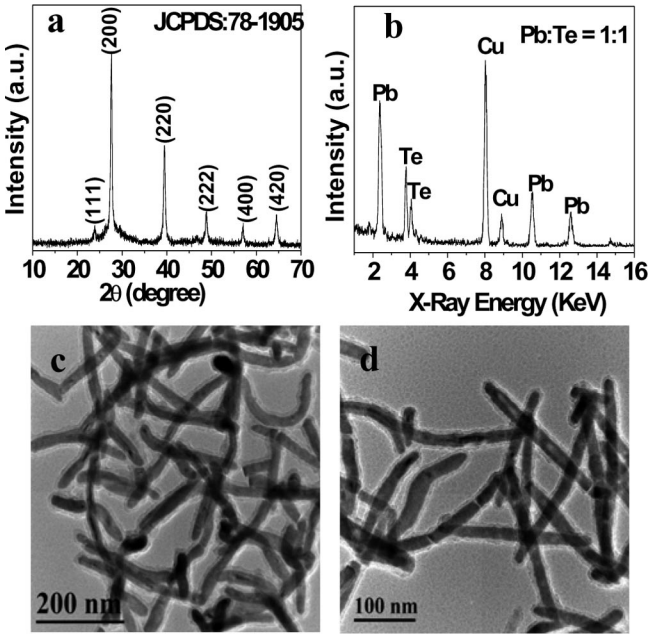


Figure 1. (a) XRD pattern, (b) EDS spectrum, and (c and d) TEM images of as-prepared PbTe nanowires.

Figure 2a shows the XRD pattern of as-synthesized CdTe nanowires. The diffraction peaks confirm that single-phase CdTe with a cubic structure (JCPDS No. 15–0770) was obtained. The EDS shown in Figure 2b indicates that the product was composed of Cd and Te elements with an atomic ratio of approximately 1:1. TEM images shown in Figure 2c–e reveal that well-dispersed CdTe nanowires were prepared. The image with a higher magnification in Figure 2e shows a typical individual nanowire with a diameter of less than 20 nm and a length around 1 μm. The selected-area electron diffraction (SAED) pattern was taken on this nanowire and is shown in the inset of Figure 2e. The well-defined diffraction spots indicate the single-crystalline structure of the CdTe nanowire. A HRTEM image of the CdTe nanowire was shown in Figure 2f, which confirms its single crystalline structure. A lattice spacing of 0.373 nm along the nanowire axis was obtained, indicating that the growth of the nanowire was along the [111] direction.

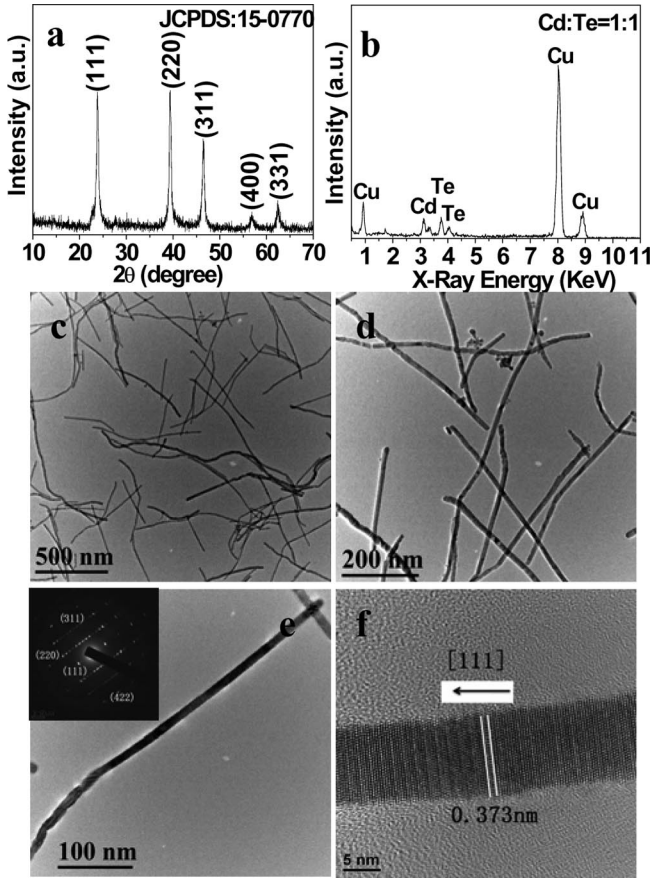


Figure 2. (a) XRD pattern, (b) EDS spectrum, and (c–e) TEM and (f) HRTEM images of as-prepared CdTe nanowires. The inset of (e) shows an SAED pattern from a single nanowire.

The morphologies of the $Bi_2Te_3$ and $Cu_7Te_4$ nanostructures are significantly different from those of PbTe and CdTe nanowires although the same growth procedures have been used. The XRD pattern, EDS, and TEM images of the as-grown $Bi_2Te_3$ nanostructures are shown in Figure 3. The diffraction peaks in Figure 3a can be well indexed to a single phase of $Bi_2Te_3$ with a hexagonal structure (JCPDS No.15–0863). The EDS measurements further verify that the atomic ratio of Bi to Te is 2:3.

The as-prepared $Bi_2Te_3$ samples exhibit serrate-like 1D nanostructures, as shown in the TEM images of Figure 3c–f. They still exhibit a nanowire-like morphology with an average diameter around 100 to 200 nm and lengths in the micrometer range. The surface of the nanostructures is very rough. The TEM images with higher magnification exhibit that each of the 1D nanostructure is actually composed of nanosheet assemblies with the nanosheets aligned perpendicular to the axis of the 1D nanostructure. The thickness of the nanosheets is about 10 to 15 nm. During growth, these nanosheets stack together and form the special 1D

  

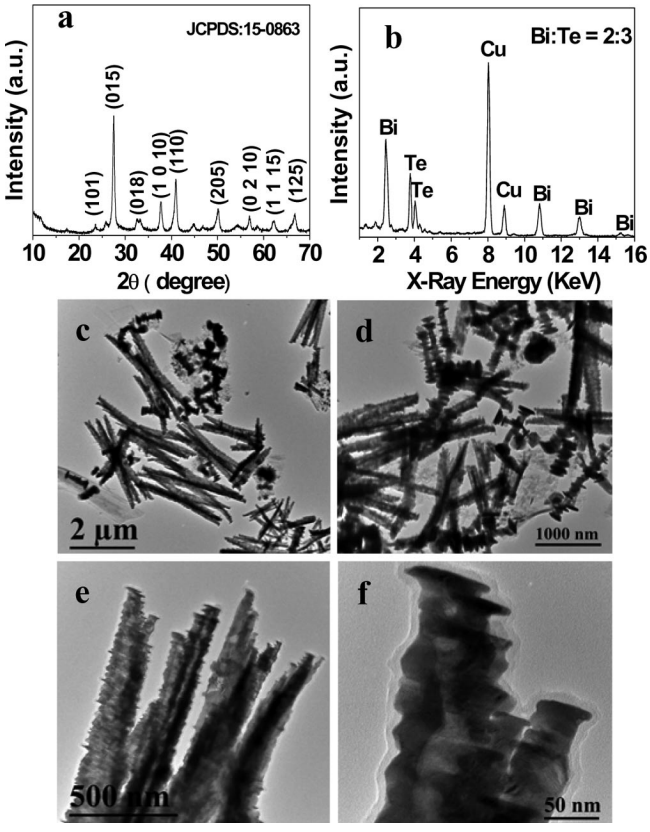


Figure 3. (a) XRD pattern, (b) EDS spectrum, and (c–f) TEM images of as-prepared $Bi_2Te_3$ nanostructures.

nanostructures. This growth mode differs from those of the PbTe and CdTe nanowires.

$Cu_7Te_4$ nanostructures were also successfully synthesized by using the aforementioned method, and their structural analysis is shown in Figure 4. A hexagonal structure of $Cu_7Te_4$ (JCPDS No.18–0456) was obtained as evidenced by the XRD measurement (Figure 4a). The TEM micrographs displayed in Figure 4b,c exhibit that the as-prepared sample consists of nanospheres with a uniform size distribution. The diameters of the spheres are around 200 nm. A magnified image shown in Figure 4c suggests that these nanospheres are solid and composed of nanoparticles with much smaller sizes. The inset of Figure 4c shows a SAED pattern taken from a single nanosphere. A combination of diffraction rings and spots were obtained from the $Cu_7Te_4$ nanospheres, indicating the polycrystalline nature of the nanospheres. This observation is consistent with the TEM observation that a nanosphere contains many smaller nanoparticles. The discontinuous rings and diffraction spots indicate that the nanoparticles are oriented along crystalline directions such as [110], [220], [302], and [103].

Figure 5 shows the XRD patterns and TEM images of cobalt telluride ($CoTe_2$) nanostructures prepared in the absence of polyvinyl pyrrolidone (PVP). It can be seen that the diffraction peaks from $CoTe_2$ with an orthorhombic structure are observed in the XRD pattern, consistent with the literature data (JCPDS: 74–0245). A weak peak at 27.65° was observed and ascribed to Te with a hexagonal

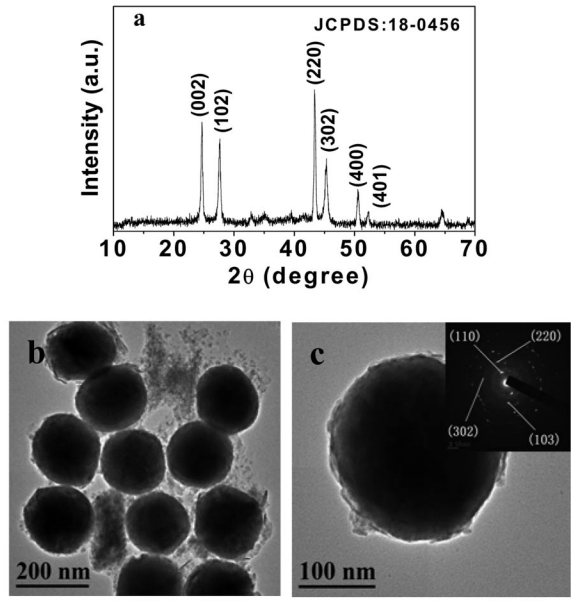


Figure 4. (a) XRD pattern and (b and c) TEM images of as-prepared $Cu_7Te_4$ nanospheres. The inset of (c) is an SAED pattern from a single nanosphere.

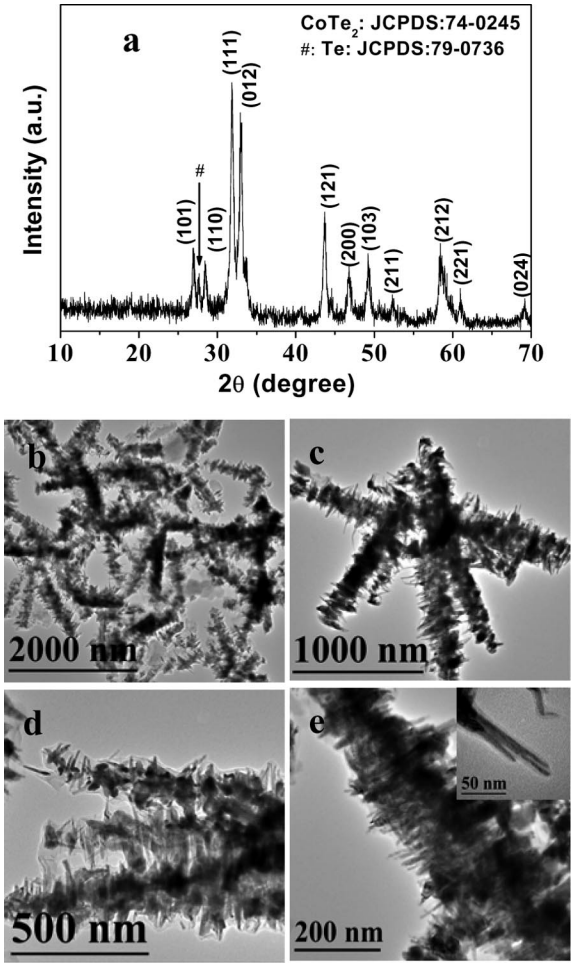


Figure 5. (a) XRD pattern and (b–e) TEM images of saw-like $CoTe_2$ nanostructures prepared in the absence of PVP.

  

structure (JCPDS: 79–0736). This observation indicates that a small amount of Te is present as impurities in the $CoTe_2$ nanostructures. The as-prepared $CoTe_2$ samples exhibit saw-like 1D nanostructures, as can be seen from the TEM images of Figure 5b–e. High-magnification images indicate that a large amount of small nanorods aligns perpendicular to the growth axis, forming the 1D nanostructures with lengths in the micrometer range. The inset of Figure 5e reveals that the small nanorods have diameters of only several nanometers and lengths of tens to hundreds nanometers. The morphology of the saw-like $CoTe_2$ 1D nanostructures is to some extent similar to that of serrate-like $Bi_2Te_3$ nanostructures. However, $CoTe_2$ and $Bi_2Te_3$ nanostructures, respectively, use $CoTe_2$ nanorods and $Bi_2Te_3$ nanosheets as their building blocks to the 1D nanostructures. Figure 6 shows $CoTe_2$ nanostructures prepared in the presence of PVP, which indicates the influence of PVP on the morphology of as-prepared $CoTe_2$. From Figure 6 one can see that a mixture containing nanowires, nanorods, and nanoparticles was obtained, which is different from the saw-like 1D nanostructures assembled with nanorods obtained without PVP (Figure 5).

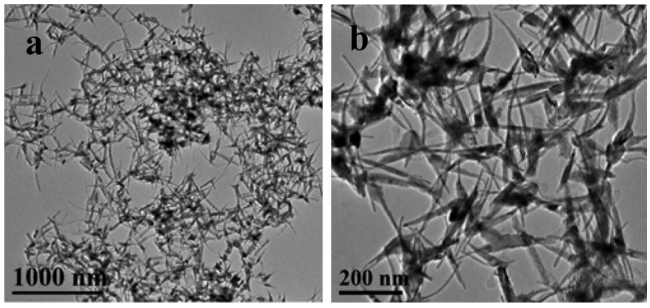


Figure 6. TEM images of $CoTe_2$ nanostructures synthesized in the presence of PVP.

## Growth Mechanism

It is known that ascorbic acid is a weak reducing agent[24–26] and would slowly reduce $Te^{4+}$ to Te in solution at certain temperatures.[27] In addition, ethylene glycol (EG) has been used as a reducing agent for the synthesis of Te nanowires[28] and nanotubes,[29] $Sb_2Te_3$ nanoforks,[30] PbSe nanotubes,[31] and $Bi_2Te_3$ hollow nanospheres.[32] On the basis of literature data and the experimental results obtained in this study, possible reaction mechanisms for the formation of 1D metal telluride $M_mTe_n$ (M = Cd, Pb, Bi, or Co) nanostructures are discussed in the following paragraphs.

The growth mechanisms of PbTe, CdTe, and $Bi_2Te_3$ 1D nanostructures are sketched in Scheme 1. In the early growth stage, soluble $Na_2TeO_3$ is dissociated into $TeO_3^{2-}$ and $Na^+$ ions in water, and then reacts with $M^{n+}$ to form $M_m(TeO_3)_n$ precipitates, which are insoluble in water at room temperature. When the mixtures of the reaction agents were solvothermally heated to a high temperature such as 200 °C, $M_m(TeO_3)_n$ precipitates began to dissolve. Then, $H^+$ ions, resulting from the ionization of ascorbic acid, reacted with $TeO_3^{2-}$ to generate $TeO_2$. Again, $TeO_2$ is insoluble in water at room temperature but dissolvable at high temperature.[27] As a weak reducing agent, ascorbic acid can reduce $Te^{4+}$ to Te in solution, which results in the growth of Te nanowires. These Te nuclei are highly reactive in the presence of EG at temperatures around 200 °C. The transformation reaction from Te to $M_mTe_n$ initially takes place on the surface of the newly formed Te nanowires because of their contact directly with $M^{n+}$ and EG, resulting in the growth of a thin sheath of $M_mTe_n$ on the Te nanowire cores. With the increase in reaction time, the Te nanowire cores were eventually converted into $M_mTe_n$ as a result of the inward diffusion of the reactants. Shi et al.[30] reported that EG served as a reducing agent for the reduction of Te to $Te^{2-}$ in the synthesis of $Sb_2Te_3$ nanoforks, which is similar to the initial reaction process on Te surfaces proposed in this study.

The chemical reactions involved in this process are shown as follows (with $Pb^{2+}$ as an example):

$$2H^+ + TeO_3^{2-} \rightarrow TeO_2 + H_2O$$

$$TeO_2 + C_6H_8O_6 \rightarrow Te + C_6H_4O_6 + 2H_2O$$

$$Pb^{2+} + Te + C_2H_6O_2 \rightarrow PbTe + C_2H_4O_2 + 2H^+$$

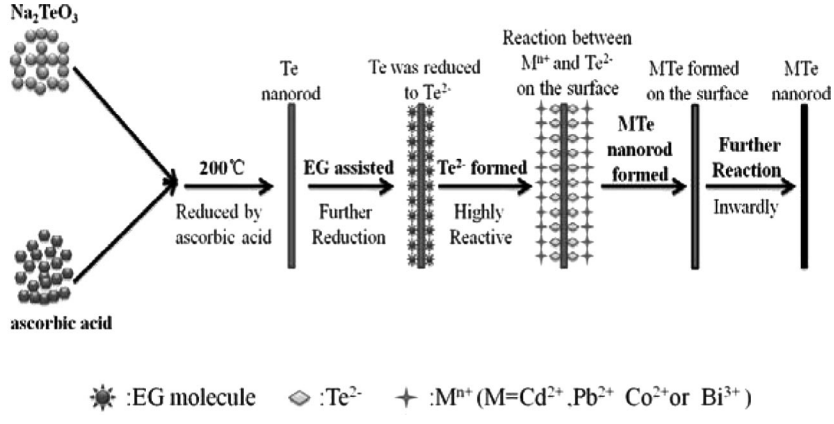


Scheme 1. Illustration for the formation of PbTe, CdTe, and $Bi_2Te_3$ 1D nanostructures with different morphologies.

  

The formation of $CoTe_2$ 1D saw-like nanostructures is shown in Scheme 2. The $CoTe_2$ nanorods are first grown in solution. Then, the $CoTe_2$ nanorods experience an oriented self-assembly process, in which the nanorods align themselves to form nanorod arrays perpendicular to the growth direction of the 1D nanostructures. In a previous paper, we reported the preparation of ZnS nanospheres assembled from nanorods by using L-cysteine as the sulfur source in a solvothermal process, and the growth mechanism of the nanostructured spheres assembled from nanorods was proposed.[33] Because the reaction system adopted here is totally different from that of our previous work, the morphologies of the nanostructures and the growth mechanisms are also different from the growth of ZnS nanostructures.

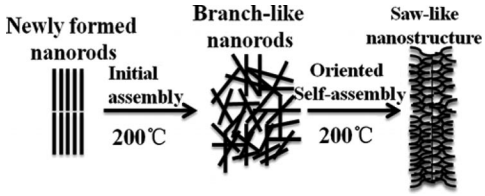


Scheme 2. Illustration for the formation of $CoTe_2$ saw-like nanostructures.

## Optical Properties

To examine the optical properties of the yielded $CoTe_2$, CdTe, and $Cu_7Te_4$ nanostructures, photoluminescence (PL) and UV/Vis absorption measurements were performed at room temperature. A PL spectrum of $CoTe_2$ nanostructures is shown in Figure 7. A broad PL emission centered at 557 nm of the as-prepared $CoTe_2$ nanostructures was observed. Some metal tellurides exhibit PL at room temperature such as CdTe. However, it is generally hard to observe PL in transition metal tellurides like $CoTe_2$ as a result of magnetic interactions, which quench optical radiation. Nonetheless, the properties of the materials may dramatically change when their size is in the range of nanometers. Quantum confinement and surface effects become prominent with such small dimensions. Quantum confinement effects may induce delocalized states and enhance the electron-phonon interaction, leading to optical transitions in the nanostructures that are not present in the bulk materials. The reduction in the magnetic interaction may occur on the nanometer scale and result in the formation of nonmagnetic covalent bonds. The observed PL in $CoTe_2$ nanostructures may result from a combination of these effects at the extremely small size. Growth of other impurities such as Te in $CoTe_2$ as observed by XRD may also contribute to optical radiation. The very broad emission band seems to suggest that surface states and defects could be majorly responsible for the observed PL spectra. Further investigations are still needed to fully understand the PL mechanism.

Figure 8 shows the UV/Vis absorption spectra taken on $Cu_7Te_4$ and CdTe nanostructures. The $Cu_7Te_4$ nanospheres and CdTe nanowires were ultrasonically dispersed in ethanol for absorption measurements. The absorption spectrum

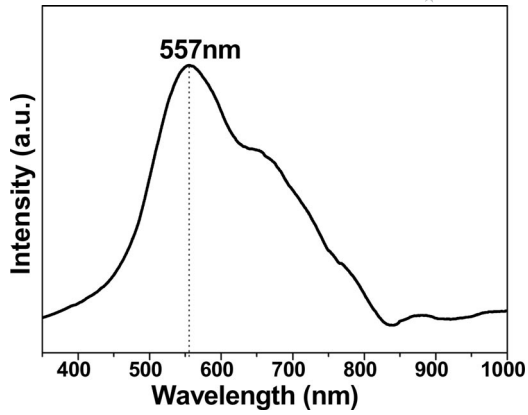


Figure 7. Photoluminescence spectrum of saw-like $CoTe_2$ nanostructures at room temperature.

of $Cu_7Te_4$ nanospheres dispersed in ethanol exhibits a distinctive absorption peak at about 213 nm (Figure 8a). It is not clear what causes this absorption peak. To the best of our knowledge, it has not been reported so far. Considering the nanospheres are composed of much smaller nanoparticles, the size effect of these nanoparticles might be responsible for the UV absorption. It has been reported that the absorption of spherical nanoparticles of both metals and semiconductors can be enhanced and the absorption bands shift to short wavelengths at a smaller particle size.[34,35]

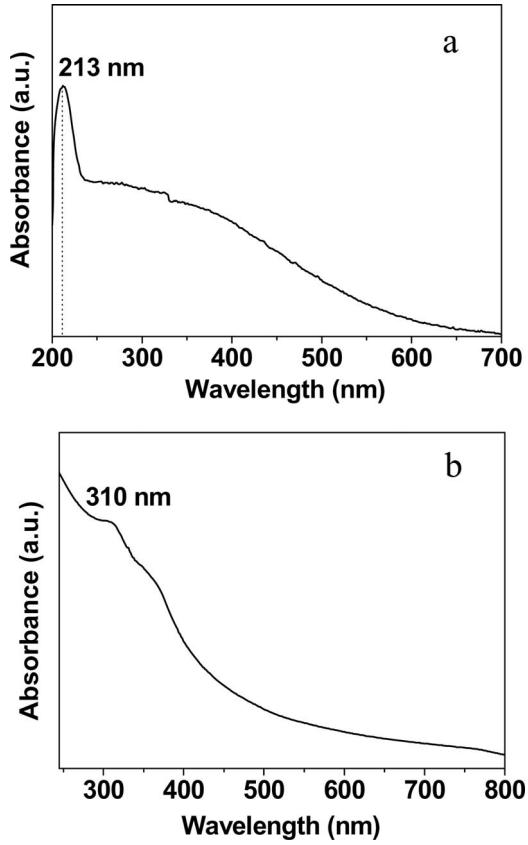


Figure 8. UV/Vis absorption spectra of (a) $Cu_7Te_4$ nanospheres and (b) CdTe nanowires at room temperature.

  

It is known that CdTe is a semiconductor with a direct band gap ($E_g$) of 1.56 eV at 300 K. The intrinsic absorption occurs around 796 nm.[21] A similar result on CdTe nanowires dispersed in solution was recently reported by Liang et al.[14] The as-prepared CdTe nanowires show an absorption in a wide range of wavelengths from about 280 to 800 nm (Figure 8b), which may be potentially useful for solar cell applications. The lack of a pronounced band edge absorption may result from quantum confinement effects, which cause the band gap to shift to higher energies in the nanowires. In combination with a size distribution of the nanowires, the band edge absorption can be smeared in the spectrum.

## Conclusions

In summary, we have developed a general and facile surfactant-assisted solvothermal route for the synthesis of various metal telluride nanostructures (PbTe, CdTe, $CoTe_2$, $Bi_2Te_3$, and $Cu_7Te_4$) by using a corresponding metal salt, $Na_2TeO_3$, ascorbic acid, and PVP in mixed solvents of EG and water. A variety of morphologies were observed in these tellurides, including PbTe and CdTe nanowires, $Bi_2Te_3$ serrate-like 1D nanostructures assembled with nanosheets, $Cu_7Te_4$ nanospheres, and $CoTe_2$ saw-like nanostructures assembled with nanorods. It is expected that this method may be extended to the synthesis of other metal telluride nanostructures. Optical properties of the telluride nanostructures were also investigated. A few interesting observations were obtained, including visible photoluminescence of $CoTe_2$ nanostructures and UV/Vis absorption of $Cu_7Te_4$ nanospheres and CdTe nanowires. The possible mechanisms were discussed in terms of size and surface effects in these nanomaterials.

## Experimental Section

**Chemicals:** $CdCl_2·2.5H_2O$, $Pb(NO_3)_2$, $Co(NO_3)_2·6H_2O$, $CuCl_2·2H_2O$, $Bi(NO_3)_3·5H_2O$, $Na_2TeO_3$, ascorbic acid, and ethylene glycol (EG) were purchased and used as received without further purification.

**Typical Procedure for Fabricating PbTe, CdTe, $Bi_2Te_3$, and $Cu_7Te_4$ Nanostructures:** $Pb(NO_3)_2$ (0.331 g), $CdCl_2·2.5H_2O$ (0.228 g), $Bi(NO_3)_3·5H_2O$ (0.485 g), or $CuCl_2·2H_2O$ (0.340 g) was dissolved in deionized water (50 mL). Then, $Na_2TeO_3$ (0.22 g) was added and a precipitate of $PbTeO_3$, $CdTeO_3$, $Bi_2(TeO_3)_3$, or $CuTeO_3$ appeared immediately. After stirring for about 10 min, ascorbic acid (1 g), PVP (1 g), and EG (30 mL) were added. The mixture was stirred for 20 min to form a well-dispersed turbid solution. The suspension was put into a Teflon-lined stainless steel autoclave of 100-mL capacity and sealed and heated at 200 °C for 24 h. After heating, the autoclave was taken out and cooled to room temperature in air naturally. The black product was collected by centrifugation, washed with deionized water and absolute ethanol three times (except for $Cu_7Te_4$), and then dried at 60 °C in vacuo. The $Cu_7Te_4$ product could not be obtained by regular centrifugation, so the $Cu_7Te_4$ suspension was heated to 100 °C in a beaker to evaporate the water. When about 20 mL was left, heating was terminated, and the solution was allowed to cool down to room temperature naturally; then, acetone (50 mL) and absolute ethanol (50 mL) were added. The resulting suspension was kept stationary for 3 h. Then, the suspension was centrifuged, washed with water and absolute ethanol three times, and then dried at 60 °C in vacuo.

**Synthesis of $CoTe_2$ Nanostructures:** $Co(NO_3)_2·6H_2O$ (0.15 g) and $Na_2TeO_3$ (0.11 g) were dissolved in deionized water (15 mL). Afterwards, ascorbic acid (1 g) and EG (20 mL) were added. It should be noted that the cobalt telluride ($CoTe_2$) nanostructures were prepared in the absence of the surfactant PVP. After stirring for 20 min, the mixture was put into a Teflon-lined stainless steel autoclave of 50-mL capacity and sealed and heated at 200 °C for 12 h. The comparison experiment for the synthesis of $CoTe_2$ nanostructures was carried out by using PVP (0.6 g) while keeping other conditions the same as those described above.

**Characterizations:** X-ray powder diffraction (XRD) patterns were recorded with a Rigaku D/MAX 2550V X-ray diffractometer with Cu-$K_\alpha$ radiation ($\lambda$ = 1.54178 Å) and a graphite monochromator. Transmission electron microscopy (TEM) images, high-resolution TEM (HRTEM), and energy dispersive spectroscopy (EDS) were performed with a JEOL JEM-2100F field-emission transmission electron microscope. The UV/Vis spectra were recorded with a spectrophotometer (UV-2300, Techcomp) at room temperature. Photoluminescence was excited by the 325 nm line of a He-Cd laser. The emission light was focused onto the entrance of a monochromator and recorded by a CCD detector.

## Acknowledgments

This work was financially supported by the National Natural Science Foundation of China (50772124, 50821004), the Science and Technology Commission of Shanghai (0852 nm05800), and the Opening Project of State Key Laboratory of High Performance Ceramics and Superfine Microstructure (SKL200901SIC).

[1] A. P. Alivisatos, *Science* **1996**, *271*, 933–937.
[2] T. M. Tritt, *Science* **1999**, *283*, 804–805.
[3] K. F. Hsu, S. Loo, F. Guo, W. Chen, J. S. Dyck, C. Uher, T. Hogan, E. K. Polychroniadis, M. G. Kanatzidis, *Science* **2004**, *303*, 818–821.
[4] M. S. Dresselhaus, G. Dresselhaus, X. Sun, Z. Zhang, S. B. Cronin, T. Koga, J. Y. Ying, G. Chen, *Microscale Thermophys. Eng.* **1999**, *3*, 89–100.
[5] J. Ham, W. Shim, D. H. Kim, S. Lee, J. Roh, S. W. Sohn, K. H. Oh, P. W. Voorhees, W. Lee, *Nano Lett.* **2009**, *9*, 2867–2872.
[6] I. Gur, N. A. Fromer, M. L. Geier, A. P. Alivisatos, *Science* **2005**, *310*, 462–465.
[7] N. P. Gaponik, D. V. Talapin, A. L. Rogach, A. Eychmuller, *J. Mater. Chem.* **2000**, *10*, 2163–2166.
[8] S. P. Wang, N. Mamedova, N. A. Kotov, W. Chen, J. Studer, *Nano Lett.* **2002**, *2*, 817–822.
[9] P. E. Trudeau, M. Sheldon, V. Altoe, A. P. Alivisatos, *Nano Lett.* **2008**, *8*, 1936–1939.
[10] P. Bottcher, *Angew. Chem. Int. Ed. Engl.* **1988**, *27*, 759–772.
[11] B. Li, Y. Xie, J. X. Huang, H. L. Su, Y. T. Qian, *J. Solid State Chem.* **1999**, *146*, 47–50.
[12] B. Li, Y. Xie, J. X. Huang, Y. Liu, Y. T. Qian, *Chem. Mater.* **2000**, *12*, 2614–2616.
[13] Y. Xie, B. Li, H. L. Su, X. M. Liu, Y. T. Qian, *Nanostruct. Mater.* **1999**, *11*, 539–544.
[14] H. W. Liang, S. Liu, Q. S. Wu, S. H. Yu, *Inorg. Chem.* **2009**, *48*, 4927–4933.
[15] G. A. Tai, W. L. Guo, Z. H. Zhang, *Cryst. Growth Des.* **2008**, *8*, 3878–3878.

  

[16] P. F. Zuo, S. Y. Zhang, B. K. Jin, Y. P. Tian, J. X. Yang, *J. Phys. Chem. C* **2008**, *112*, 14825–14829.
[17] G. Tai, B. Zhou, W. L. Guo, *J. Phys. Chem. C* **2008**, *112*, 11314–11318.
[18] P. Kumar, K. Singh, *Cryst. Growth Des.* **2009**, *9*, 3089–3094.
[19] F. Y. Li, C. G. Hu, Y. F. Xiong, B. Y. Wan, W. Yan, M. C. Zhang, *J. Phys. Chem. C* **2008**, *112*, 16130–16133.
[20] Q. Peng, Y. J. Dong, Y. D. Li, *Inorg. Chem.* **2003**, *42*, 2174–2175.
[21] H. Gong, X. P. Hao, C. Gao, Y. Z. Wu, J. Du, X. G. Xu, M. H. Jiang, *Nanotechnology* **2008**, *19*, 445603.
[22] A. M. Qin, Y. P. Fang, P. F. Tao, J. Y. Zhang, C. Y. Su, *Inorg. Chem.* **2007**, *46*, 7403–7409.
[23] H. Tong, Y. J. Zhu, L. X. Yang, L. Li, L. Zhang, *Angew. Chem. Int. Ed.* **2006**, *45*, 7739–7742.
[24] N. R. Jana, L. Gearheart, C. J. Murphy, *Chem. Commun.* **2001**, 617–618.
[25] N. R. Jana, L. Gearheart, C. J. Murphy, *J. Phys. Chem. B* **2001**, *105*, 4065–4067.
[26] N. R. Jana, L. Gearheart, C. J. Murphy, *Adv. Mater.* **2001**, *13*, 1389–1393.
[27] G. C. Xi, Y. K. Liu, X. Q. Wang, X. Y. Liu, Y. Y. Peng, Y. T. Qian, *Cryst. Growth Des.* **2006**, *6*, 2567–2570.
[28] Y. J. Zhu, X. L. Hu, *Chem. Lett.* **2004**, *33*, 760–761.
[29] B. Mayers, Y. N. Xia, *Adv. Mater.* **2002**, *14*, 279–282.
[30] S. F. Shi, M. H. Cao, C. W. Hu, *Cryst. Growth Des.* **2009**, *9*, 2057–2060.
[31] T. Huang, L. M. Qi, *Nanotechnology* **2009**, *20*, 025606.
[32] Y. Jiang, Y. J. Zhu, L. D. Chen, *Chem. Lett.* **2007**, *36*, 382–383.
[33] H. Tong, Y. J. Zhu, L. X. Yang, L. Li, L. Zhang, J. Chang, L. Q. An, S. W. Wang, *J. Phys. Chem. C* **2007**, *111*, 3893–3900.
[34] Z. B. Li, Y. D. Deng, B. Shen, W. B. Hu, *J. Phys. D: Appl. Phys.* **2009**, *42*.
[35] F. Wang, G. Y. Xu, Z. Q. Zhang, X. Xin, *Eur. J. Inorg. Chem.* **2006**, 109–114.

Received: March 3, 2010
Published Online: May 19, 2010

  